Electromagnons in multiferroic RMn_2O_5 compounds and their microscopic origin

Electromagnons in multiferroic RMn$_2$O$_5$ compounds and their microscopic origin

A B Sushkov[1]**, M Mostovoy**[2]**, R Valdés Aguilar**[1]**, S-W Cheong**[3] **and H D Drew**[1]

[1] Materials Research Science and Engineering Center, University of Maryland, College Park, MD 20742, USA
[2] Zernike Institute for Advanced Materials, University of Groningen, NL-9747 AG Groningen, The Netherlands
[3] Rutgers Center for Emergent Materials and Department of Physics and Astronomy, Rutgers University, Piscataway, NJ 08854, USA

E-mail: sushkov@umd.edu

Abstract

We summarize the existing experimental data on electromagnons in multiferroic RMn$_2$O$_5$ compounds, where R denotes a rare earth ion, Y or Bi, and discuss a realistic microscopic model of these materials based on the assumption that the microscopic mechanism of magnetically induced ferroelectricity and electromagnon absorption relies entirely on the isotropic Heisenberg exchange and magnetostrictive coupling of spins to a polar lattice mode and does not involve relativistic effects. This model explains many magnetic and optical properties of RMn$_2$O$_5$ manganites, such as the spin re-orientation transition, magnetically induced polarization, appearance of the electromagnon peak in the non-collinear spin state and the polarization of light for which this peak is observed. We compare experimental and theoretical results on electromagnons in RMn$_2$O$_5$ and RMnO$_3$ compounds.

(Some figures in this article are in colour only in the electronic version)

1. Introduction

Multiferroic materials that exhibit simultaneous magnetic and ferroelectric order have attracted much attention recently because of the fundamental interest of systems with coupled order parameters and because of their potential for cross electric and magnetic functionality [1–7]. Many recently discovered multiferroics, e.g. TbMnO$_3$ [8], TbMn$_2$O$_5$ [9] and Ni$_3$V$_2$O$_8$ [10], are improper ferroelectrics in which the electric polarization is induced by spin ordering. These materials show striking cross-coupling effects such as magnetic field induced polarization switching [8, 9] and giant magnetocapacitance [11] and a strong coupling between spin and lattice excitations that leads to electric dipole excitation of magnons, or electromagnons [1, 12–14], which is the subject of this paper. The fundamental interest in multiferroicity also derives from the strong interplay between magnetic frustration, ferroelectric order and unusual symmetry breaking in phase transformations that characterize these materials [6, 15].

The known microscopic mechanisms of magnetically induced ferroelectricity include lattice distortion (exchange striction) and redistribution of electron density in response to spin ordering. Such processes occur locally in all magnetic materials. However, only when a spin ordering breaks inversion symmetry do these local electric dipoles add into a macroscopic electric polarization. Spin orders that break inversion symmetry are rare and the best systems to look for them are frustrated magnets, where competing interactions and the geometry of spin lattice favour unconventional magnetic states. In most of the recently discovered multiferroic materials, such as TbMnO$_3$, Ni$_3$V$_2$O$_8$, MnWO$_4$ and CuO, competing interactions force spins to form a cycloidal spiral. This non-collinear spin order breaks inversion symmetry and activates antisymmetric Dzyaloshinskii–Moriya interactions proportional to the cross-product of spins, $S_1 \times S_2$ [16]. The concomitant lattice and electronic distortion induces electric polarization [17–19].

When inversion symmetry is broken by a collinear magnetic ordering the strongest spin interaction that can

shift ions and polarize electronic clouds is the symmetric Heisenberg exchange, proportional to the scalar product of spins, $S_1 \cdot S_2$. This mechanism was proposed to explain multiferroic properties of RMn_2O_5, where R denotes a rare earth ion, Y or Bi, and orthorhombic manganites showing the E-type antiferromagnetic ordering [20–22].

These two microscopic mechanisms of magnetically induced ferroelectricity give rise to two different forms of phenomenological magnetoelectric coupling: electric polarization induced by a low-pitch spiral is described by the third-order coupling term $P(L_1 \partial L_2 - L_2 \partial L_1)$, where P is the electric polarization and $L_{1,2}$ are magnetic order parameters describing the sinusoidal and cosinusoidal components of the spiral [23, 24], while the coupling working in collinear spin states has the form $P(L_1^2 - L_2^2)$, where L_1 and L_2 are components of a two-dimensional irreducible representation describing magnetic states with opposite electric polarizations [25, 20, 22].

The magnetoelectric interactions that induce electric polarization in magnets can also couple oscillations of magnetization to polar lattice vibrations. The oscillations of polarization at magnon frequency and vice versa give rise to dynamic magnetoelectric effects, such as electromagnon excitations. In the usual magnets, an oscillating electric field of photons can excite a three-particle continuum consisting of two magnons and one phonon [26]. This process results from the fourth-order spin–lattice coupling (see figure 1(a)). The third-order couplings in multiferroics, discussed above, make possible photo-excitation of the two-magnon continuum without a phonon ('charged magnons' [27]) shown in figure 1(b). Replacing one of the magnons by the static modulation of spin density appearing in the ordered spin state, we obtain a process that converts a photon into a single magnon, which is the electromagnon (see figure 1(c)). This process is usually mediated by a polar phonon linearly coupled to both magnons and light, which for low-frequency phonons can lead to a resonant enhancement of the photo-excitation of electromagnons.

As there are two possible contributions to the polarization— from ionic displacements and from electronic density redistribution—one can think of two corresponding electric contributions to the electromagnon—from phonons and from electronic excitations. This means a transfer of the electric dipole spectral weight from phonons ($\hbar\omega \sim$ 10–100 meV) and/or electronic excitations ($\hbar\omega \sim$ 2 eV) down to magnons ($\hbar\omega \sim$ 1–5 meV). Such a transfer, in turn, leads to a step-like anomaly in the temperature dependence of the dielectric constant. Current research on electromagnons, including this paper, is focused mainly on magnon–phonon coupling while the magnon–electron aspect is much less explored as it is generally expected to be weak because of the large energy difference between the electronic excitations and the magnetic excitations.

The possibility of electromagnon excitations in multiferroics has long been anticipated theoretically [1], but only recently were they observed in experiment. Pimenov *et al* [12] reported observations of electric active modes at magnon frequencies in $GdMnO_3$ and $TbMnO_3$ which exist only in some magnetically ordered phases and can be suppressed by the
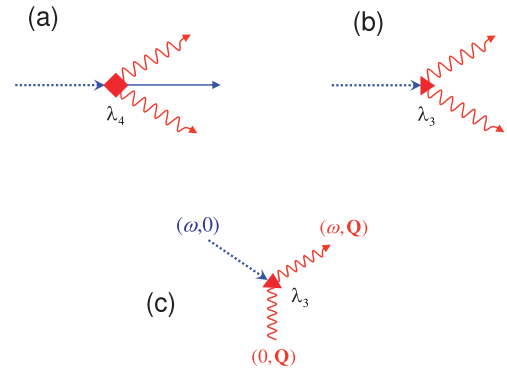

Figure 1. Feynman diagrams describing photo-excitation of magnons by the electric field of light (here photon and phonon are represented, respectively, by dashed and solid lines, while the wavy line corresponds to magnon): (a) photo-excitation of two magnons and one phonon via the fourth-order magnetoelectric coupling (the Lorenzana–Sawatzky mechanism), (b) excitation of the two-magnon continuum via the third-order magnetoelectric coupling ('charged magnons') and (c) photo-excitation of a single magnon (electromagnon) due to the third-order magnetoelectric coupling, where a photon with frequency ω and zero wavevector scatters off the static spin modulation with the wavevector Q producing a magnon with the same wavevector and frequency ω.

magnetic field. Further, they found in $GdMnO_3$ the spectral weight transfer from the lowest frequency phonon down to the electromagnon mode [28]. Sushkov *et al* [13] reported observation of electromagnons in YMn_2O_5 and $TbMn_2O_5$. Electromagnons in both these RMn_2O_5 compounds have very similar spectra and exist only in magnetic ferroelectric phases that proves their magnetic origin. Valdés Aguilar *et al* [29] showed that electromagnon absorption in $Eu_{0.75}Y_{0.25}MnO_3$ occurs over a broad band with two peaks, both of which exist only in the magnetic ferroelectric phase below 30 K. Pimenov *et al* [30] explored a composition set $Eu_{1-x}Y_xMnO_3$ for $0 \leqslant x \leqslant 0.5$ and confirmed the main features of electromagnons in $RMnO_3$. Kida *et al* [31] found out that the electromagnon polarization in $DyMnO_3$ stays with the lattice when the spin plane is rotated by the external magnetic field. Electromagnons, observed so far only in non-collinear spin phases of $RMnO_3$ and RMn_2O_5 compounds, have common features for both families: they are active only in one polarization $e \parallel a$ axis for $RMnO_3$ and $e \parallel b$ axis for RMn_2O_5, where e is the electric field of light; well-defined peaks exist only in the low-temperature magnetic ferroelectric phase. A theory of electromagnons for the circular magnetic spiral was developed by Katsura *et al* [14] and its continuum version was given by de Sousa *et al* [32, 33] who applied it to describe low-energy excitations in $BiFeO_3$. Fang and Hu [34] discussed electromagnon absorption in RMn_2O_5 compounds assuming Heisenberg interactions between spins.

The outstanding fundamental questions for electromagnons are the microscopic origin of these novel excitations (Heisenberg or Dzyaloshinskii–Moriya-type exchange) in the different classes of compounds ($RMnO_3$ and RMn_2O_5), the explanation of the observed selection rules, and whether electromagnons may occur in a wider range of materials. The practical issues are enhancing the magnetocapacitance effect and its temperature range and possibly applying these new excitations
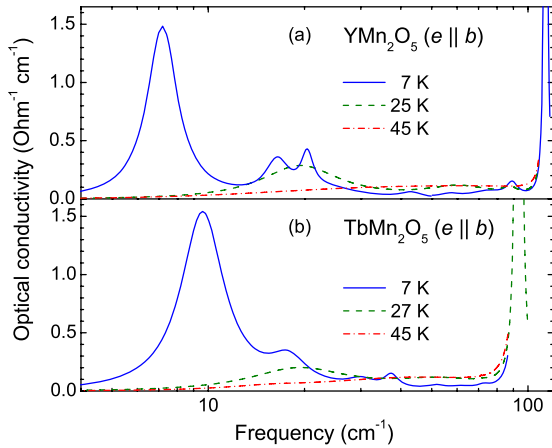
Figure 2. Optical conductivity of YMn_2O_5 and $TbMn_2O_5$ for the electric field of light $e \parallel b$ in three phases. Strong peaks at 113 and 97 cm^{-1} are the lowest phonons, other peaks are electromagnons.

to metamaterials and/or achieving a negative index of refraction in the magnon range of frequencies.

The remainder of this paper is organized as follows. In section 2, we discuss the optical absorption spectra of multiferroic YMn_2O_5 and $TbMn_2O_5$ compounds taken at different temperatures. We present experimental evidence allowing us to identify the low-frequency peaks appearing in the non-collinear phase of these materials as electromagnons. For comparison, in section 3 we present data on electromagnon peaks in the spiral multiferroic material $Eu_{0.75}Y_{0.25}MnO_3$. In section 4, we discuss a simple microscopic model of YMn_2O_5 manganites, based on isotropic Heisenberg exchange interactions between spins, with which we describe magnetic, multiferroic and optical properties of these compounds. We also briefly discuss a phenomenological description of magnetic orders and magnetoelectric coupling in RMn_2O_5 compounds based on their symmetry. In section 5, we discuss the microscopic origin of the electromagnon peaks in both RMn_2O_5 and $RMnO_3$ and how the electromagnon relates to the spontaneous polarization. Finally, we summarize our experimental and theoretical results.

2. Far-infrared spectroscopy of RMn_2O_5 compounds

The family of RMn_2O_5 compounds has long been studied [35]. Small variations of the exchange integrals with temperature lead to the complex phase diagram for this multiferroic family [36]. Earlier spectroscopic works revealed far-infrared absorption modes activated at low temperatures in $EuMn_2O_5$ [37], YMn_2O_5 [38] and $GdMn_2O_5$ [39]. Recently, we have shown that in YMn_2O_5 and $TbMn_2O_5$ strong electric dipole active modes emerge at magnon frequencies in the lowest in temperature ferroelectric phase [13]. As in the work by Pimenov *et al* [12] on $RMnO_3$ compounds, we assign these modes as electromagnons.

In figure 2, we show the optical conductivity spectra of YMn_2O_5 and $TbMn_2O_5$ at three different temperatures corresponding to three magnetic/ferroelectric phases. These spectra were obtained by fitting measured transmission
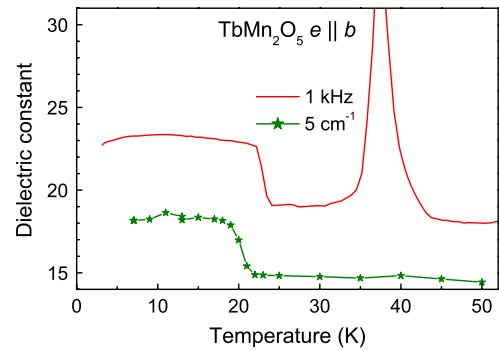

Figure 3. Dielectric constant of $TbMn_2O_5$ from fits of infrared spectra (lower curve) in comparison with kHz measurements. The whole step-like anomaly is due to electromagnons (figure 2(a), solid blue curve).

spectra [13] with the model dielectric function [40], assuming all modes to be of the electric dipole nature. The spectra measured at 7 K (blue curves) show the characteristic strong and sharp (electromagnon) absorption peaks at lowest frequencies. In this phase, the spontaneous electric polarization is relatively small and the angles between neighbouring spins along the b axis are large. The spectra measured at 25 K (green curves) have one broad absorption peak near 20 cm^{-1}. In this phase spins are almost collinear and electric polarization is large. Red curves, taken just above the Néel temperature, show a single broad absorption band below the phonon frequencies.

Identifying the low-frequency excitations as electromagnons requires addressing several questions. First, to avoid confusion with possible transitions between f-levels of rare earth ions, we have studied YMn_2O_5. The second issue is electric versus magnetic dipole (antiferromagnetic resonance) activity. We measured transmission spectra for various mutual orientations of the electric and magnetic field of light (respectively, e and h) with respect to the crystal axes and we found the absorption only for $e \parallel b \parallel P$, where P is the spontaneous polarization vector, independent of the orientation of h, which implies that the excitations are electric dipole active. Can these resonances be new phonons, activated in the low-temperature phase? We have performed shell model calculations that put the lowest phonon near 100 cm^{-1} for any reasonable parameters. Thus, we believe that we can reliably identify these low-frequency peaks as electromagnons.

Another check of the electromagnon origin of this modes is a comparison of their contribution to the step-like anomaly in the temperature dependence of ε_1, calculated using the Kramers–Kronig relation, with the measured one. Figure 3 shows such a comparison. We have chosen $TbMn_2O_5$ for this purpose because of the larger sample size and higher frequency of the electromagnon peaks. It is clear from figure 3 that the whole step-like anomaly in $\varepsilon_1(T)$ comes entirely from the sharp electromagnon peak.

The frequency and temperature behaviour, presented in figures 2 and 3, is typical for a set of RMn_2O_5 compounds: R = Er, Ho, Y, Dy, Tb, Gd and Eu [41, 42, 13, 39, 37, 43]. The appearance of electromagnon peaks as well as the ε step-like anomaly seems to be correlated with the transition into
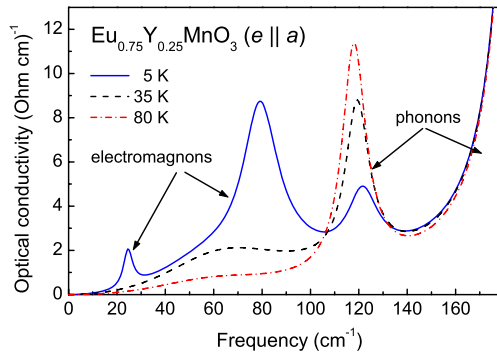
Figure 4. Optical conductivity of $Eu_{0.75}Y_{0.25}MnO_3$ for $e \parallel a$ in the ferroelectric (solid blue), the spin density wave (black dashed) and the paramagnetic (dashed–dotted red) phases. The electromagnon band consists of a broad background and two peaks.
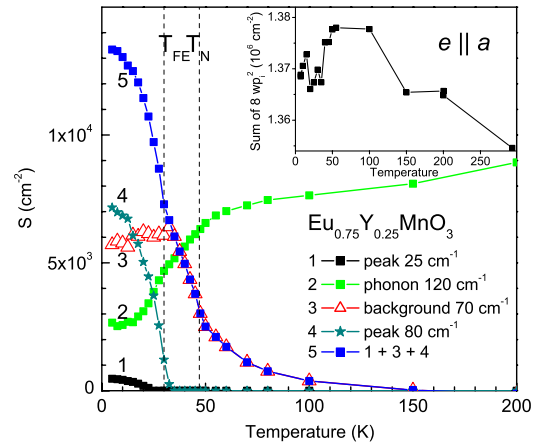

Figure 5. Spectral weight of the absorption peaks below 140 cm^{-1} in figure 4. The numbers from 1 to 5 enumerate the curves. Frequencies in the legend are the lowest temperature resonance frequencies of each mode. Inset: total spectral weight of the eight phonons above 140 cm^{-1}.

the non-collinear spin state. Notably, $BiMn_2O_5$, whose spin ordering is nearly collinear at all temperatures, shows neither the ε step-like anomaly nor electromagnon absorption [43].

An inelastic neutron scattering study of YMn_2O_5 is in progress. Preliminary data by Lee *et al* [44] show several scattering peaks in energy scans at the wavevector of the static spin structure. A strong neutron feature is observed at 1 meV in good agreement with the sharp low-frequency feature in the low-temperature infrared spectrum (figure 2(a)). Katsura *et al* [14] predict that the electromagnon originating from antisymmetric exchange has a 'transversal' polarization with respect to the spontaneous polarization: $e \perp P$. The observed polarization selection rule for electromagnons in RMn_2O_5 compounds is 'longitudinal': $e \parallel P$. We will show that such a 'longitudinal' electromagnon can be obtained in a model based on the isotropic Heisenberg exchange.

3. Far-infrared spectroscopy of $RMnO_3$

It is interesting to compare electromagnons in the two families of multiferroic manganites. We begin with $Eu_{0.75}Y_{0.25}MnO_3$—a compound that mimics lattice parameters of $TbMnO_3$ but does not have f–f transitions in the far infrared [29]. To extract the parameters of the oscillators, we fit the transmission spectra with a Lorentzian model of the dielectric constant $\varepsilon(\omega)$ for electric dipole transitions:

$$\varepsilon(\omega) = \varepsilon_\infty + \sum_j \frac{S_j}{\omega_j^2 - \omega^2 - i\omega\gamma_j} \qquad (1)$$

where ε_∞ is the high-frequency dielectric constant, j enumerates the oscillators, S_j is the spectral weight, ω_j is the resonance frequency and γ_j is the damping rate.

Figure 4 shows optical conductivity spectra for three phases of $Eu_{0.75}Y_{0.25}MnO_3$. Figure 5 shows temperature dependence of the fitted parameter S_j (spectral weight of the peaks in figure 4). A broad absorption (electromagnon) band exists well above the Néel temperature 47 K (red curve in figure 4 and curve 3 in figure 5). Upon cooling, the spectral weight S of this broad band is growing down to $T_{FE} = 30$ K and stays at this level at lower temperatures. Such a

behaviour of the background can be seen from the spectra— the absorption at 40 cm^{-1}, the frequency least affected by two absorption peaks, stays constant at all $T < T_{FE}$. This absorption produces smooth growth of the $\varepsilon_a(T)$ at $T_{FE} < T$. $T_N = 47$ K is the inflection point of curve 3 which is evidence for the magnetic origin of this low-frequency broad electric absorption. Two electromagnon peaks emerge sharply at the T_{FE} (blue curve in figure 4 and curves 1 and 4 in figure 5). They produce all further growth of the $\varepsilon_a(T)$ at $T < T_{FE}$. The electromagnon spectrum of $TbMnO_3$ is very similar to that of $Eu_{0.75}Y_{0.25}MnO_3$, except the large electromagnon peak is at 60 instead of 80 cm^{-1} [43].

It is also interesting to follow the temperature dependence of the redistribution of the electric dipole spectral weight S. Since electromagnons result from a small admixture of phonons to magnons, the total spectral weight should be conserved. Comparing curves 2 and 5 in figure 5, one can estimate how much spectral weight the 120 cm^{-1} phonon is losing and how much electromagnons acquire. As electromagnons gain more spectral weight than the phonon is losing, we checked the rest of the phonon peaks for the same polarization of light. The inset in figure 5 shows that, indeed, phonons lose just enough of the spectral weight to conserve total spectral weight.

In their recent inelastic neutron scattering work, Senff *et al* [45] reported a set of modes at the incommensurate zone centre of $TbMnO_3$. The frequency of the lowest mode is equal to the frequency of the lowest infrared peak (24 cm^{-1}). We agree with Senff *et al* in assignment of this mode as an electromagnon. However, despite the satisfied polarization selection rule $e \perp P$, this is not the electromagnon predicted by Katsura *et al* [14], as we discuss below.

4. The model of RMn_2O_5

The presence of two different types of magnetic ions and geometric frustration of spin interactions give rise to

rather complex magnetic structure RMn_2O_5 compounds. Nonetheless, a number of salient properties of these materials, such as the magnetically induced electric polarization, photo-excitation of magnons as well as the spin re-orientation transition, can be understood within a simplified microscopic model, which we discuss in this section. Our starting point is the assumption that multiferroic and optical properties of these materials are governed by the isotropic Heisenberg exchange, although we do include magnetic anisotropy to explain the spin re-orientation transition that has a strong effect on the low-frequency absorption spectrum. We discuss ordered spin states of the model, the mechanism of magnetoelectric coupling and calculate the optical absorption spectrum at magnon frequencies for different magnetic states.

We start by considering a single magnetic *ab* layer including Mn^{3+} and Mn^{4+} ions. The model describes interactions between the spins and their coupling to a polar phonon mode:

$$H = \tfrac{1}{2} \sum_{i,j} J_{ij}(\boldsymbol{P})(\boldsymbol{S}_i \cdot \boldsymbol{S}_j) - \tfrac{1}{2} \sum_{i\alpha} K_{i\alpha}(\boldsymbol{S}_i \cdot \hat{k}_{i\alpha})^2$$
$$- \sum_i \mu_i(\boldsymbol{S}_i \cdot \boldsymbol{H}) + V\left(\frac{\boldsymbol{P}^2}{2\chi_1^{(0)}} - \boldsymbol{P}\boldsymbol{E} - \frac{\chi_2 E^2}{2}\right). \quad (2)$$

Here the first term is the isotropic Heisenberg spin exchange, while the second term is the single-ion anisotropy. The antisymmetric Dzyaloshinskii–Moriya exchange as well as other types of anisotropic exchange interactions are not included, as in the scenario discussed below they play no role. We assume for simplicity that in the ordered state all spins lie in the *ab* plane [21] and neglect the small out-of-plane components found in recent neutron diffraction experiments on single crystals [46, 47]. Thus, the easy and intermediate magnetic axes on each Mn site ($\alpha = 1, 2$) lie in the *ab* plane, while the hard axis $\hat{k}_{i3} \parallel \hat{c}$. The third term in (2) is the interaction of spins with an applied magnetic field and the last term describes the dielectric response of the system, where $\chi_1^{(0)}$ is the 'bare' dielectric susceptibility related to the polar lattice mode (not including the magnetic contribution calculated below) and χ_2 is the remaining part of the dielectric susceptibility of non-magnetic origin. Finally, V is the system volume.

The coupling between the spins and the polar phonon mode results from the dependence of the exchange coupling on the electric polarization, which in RMn_2O_5 is parallel to the *b* axis:

$$J_{ij}(P_b) = J_{ij}(0) + J'_{ij}(0)P_b + \tfrac{1}{2}J''_{ij}(0)P_b^2 + \cdots. \quad (3)$$

The last two terms give rise to the cubic and the quartic magnetoelectric couplings.

4.1. Magnetic ordering and spin re-orientation transition

Here, we adopt the model of Chapon *et al* [21] with five exchange constants between pairs of nearest-neighbour Mn ions: J_1 and J_2 couple Mn^{4+} ions along the *c* direction, J_3 and J_5 couple the spins of neighbouring Mn^{3+} and Mn^{4+} ions and J_4 is the coupling between two neighbouring Mn^{3+} ions (see figure 6).

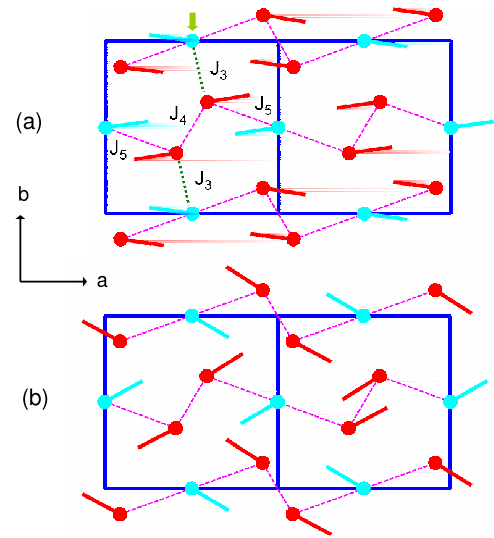**Figure 6.** Minimal energy spin configurations for $J_4 = J_5 = 40$ K and the anisotropy parameter $K_a(Mn^{3+}) = 0.6$ K for all Mn^{3+} ions (red (dark grey)) and $K_a(Mn^{4+}) = 0.1$ K for all Mn^{4+} ions (blue (light grey)). The value of the interchain coupling J_3 is -2 K for the structure in panel (a) and -4 K for the one in panel (b).

Figure 6 shows the minimal energy spin configurations obtained by the numerical minimization of the spin energy (2) on the subspace of the commensurate magnetic states with the wavevector $\boldsymbol{Q} = (1/2, 0, 0)$ for two different sets of exchange constants. The exchange constants J_4 and J_5 were chosen to be positive and large compared to other exchange constants, which gives rise to antiferromagnetic zig-zag chains along the *a* axis with nearly collinear spins (marked by dashed lines) observed in neutron experiments [21, 47].

The angle between spins in neighbouring chains sensitively depends on the ratio between the interchain coupling J_3 and the magnetic anisotropy parameters $\boldsymbol{K}_i$. We assume that the easy magnetic axis is parallel to the *a* axis. The interplay between magnetic anisotropy and interchain interaction determines the angle between spins in neighbouring antiferromagnetic chains.

We first note that, if spins in each antiferromagnetic chain would be perfectly collinear, then the interchain interactions would cancel as a result of geometric frustration. Conversely, the interchain coupling J_3 results in spin rotations, which destroy the collinearity of spins in each chain. Consider, for example, the spin of the Mn^{4+} ion, marked in figure 6(a) by an arrow. Because of a nonzero angle between spins in the neighbouring *a* chains, the interaction of the marked spin with the spin of the Mn^{3+} ion from the neighbouring chain will give rise to a rotation of the marked spin. These small spin rotations lift the frustration and lead to some energy gain due to interchain interactions. It easy to show that this energy gain is maximal when spins in neighbouring antiferromagnetic chains are orthogonal to each other. Thus, while the magnetic anisotropy favours an almost collinear spin configuration, interchain interactions favour the 90° angle between spins of neighbouring chains.

This competition gives rise to a very strong sensitivity of the angle between spins in neighbouring chains to the
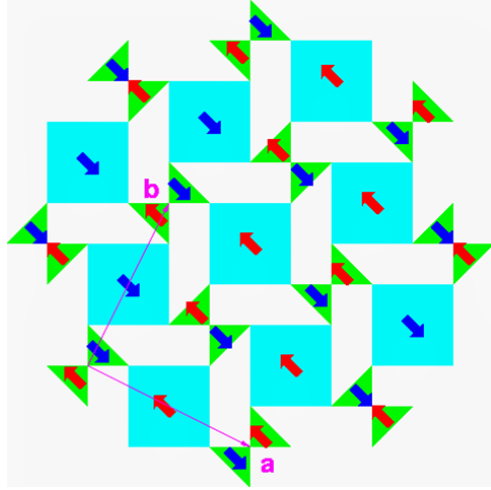
Figure 7. A cartoon of the magnetic ordering in the high-temperature collinear phase.

Figure 8. Electric polarization induced by magnetostriction along the *b* chains. The two order parameters η_1 and η_2 describe degenerate ferroelectric states with opposite directions of electric polarization.

Table 1. The coordinates of Mn ions, where $x \approx 0.41$, $y \approx 0.35$ and $z \approx 0.26$ (for BiMn$_2$O$_5$).

Mn^{3+}	Mn^{4+}
$r_1 = (x, y, 1/2)$	$r_5 = (1/2, 0, z)$
$r_2 = (-x, -y, 1/2)$	$r_6 = (1/2, 0, -z)$
$r_3 = (1/2 - x, 1/2 + y, 1/2)$	$r_7 = (0, 1/2, z)$
$r_4 = (1/2 + x, 1/2 - y, 1/2)$	$r_8 = (0, 1/2, -z)$

Table 2. Magnetic order parameters.

Mn^{3+}	Mn^{4+}
$F = S_1 + S_2 + S_3 + S_4$	$F' = S_5 + S_6 + S_7 + S_8$
$C = S_1 + S_2 - S_3 - S_4$	$C' = S_5 + S_6 - S_7 - S_8$
$G = S_1 - S_2 + S_3 - S_4$	$G' = S_5 - S_6 + S_7 - S_8$
$A = S_1 - S_2 - S_3 + S_4$	$A' = S_5 - S_6 - S_7 + S_8$

interchain coupling J_3. For weak interchain coupling $J_3 = -2$ K, this angle is relatively small and the minimal energy spin configuration shown in figure 6(a) is similar to the one observed in the high-temperature 'collinear' phase of YMn$_2$O$_5$ by Chapon *et al* [21]. A small change in J_3 from -2 to -4 K transforms the configuration shown in figure 6(a) into the one shown in figure 6(b), which may explain the spin re-orientation observed in RMn$_2$O$_5$ with R = Tb, Ho, Dy and Y, provided that the interchain coupling is temperature-dependent. Although the rotations that make spins in each chain non-collinear are barely visible, they are sufficient to produce the large changes in the spin configuration, since the magnetic anisotropy is relatively weak. In RMn$_2$O$_5$, the spin re-orientation transition is accompanied by the loss of commensurability of the spin structure in the *a* and *c* directions (which is also a consequence of magnetic frustration). This latter aspect of the transition is, however, less important for the photo-excitation of magnons, discussed below, than the re-orientation of spins.

4.2. Magnetically induced polarization

Minimizing (2) with respect to P_y, we obtain the expression for the magnetically induced electric polarization:

$$P_b \approx -\frac{\chi_1^{(0)}}{2V} \sum_{i,j} J'_{ij}(0)(S_i S_j), \qquad (4)$$

which only involves scalar products of spins.

Figures 7 and 8 show why in the high-temperature ferroelectric phase the polarization vector is oriented along the *b* axis. Figure 7 gives a simplified view of the Mn layer in the *ab* plane, in which the spins inside squares depict the spins of Mn^{4+} ions located inside oxygen octahedra, while the spins inside triangles are the spins of Mn^{3+} ions in oxygen pyramids. The nearly collinear magnetic ordering in the high-temperature ferroelectric phase consists of antiferromagnetic chains along the *a* direction.
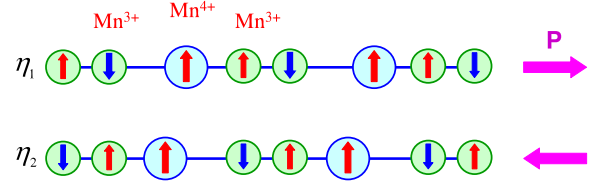
The mechanism responsible for electric polarization in this magnetic state involves, however, the ↑↑↓ and ↓↓↑ spin chains along the *b* axis, such as shown in figure 8. These chains contain the polar Mn^{4+}–Mn^{3+} bonds, connecting parallel spins, and the Mn^{3+}–Mn^{4+} bonds with opposite polarity, connecting antiparallel spins. Importantly, the charge and spin modulations in the chains have the same period, in which case the conventional exchange striction destroys the cancellation of electric dipoles of the polar bonds and induces electric polarization along the chains, as illustrated in figure 8.

This mechanism also works in the low-temperature (incommensurate) ferroelectric phase, which has the same periodicity in the *b* direction. The amplitude of the exchange striction is, however, the largest for collinear spins (see (4)), which explains the drop of the polarization at the transition to the low-temperature phase. For example, if the value of the magnetoelectric coupling $\propto J'_3 - J'_4 - J'_5$, is chosen such that the electric polarization induced by the 'high-temperature' configuration shown in figure 6(a) is 1000 μC m^{-2}, then for the 'low-temperature' configuration shown in figure 6(b) it equals 500 μC m^{-2}.

4.3. Phenomenological approach

In this subsection we discuss the phenomenological description of spin states and the magnetoelectric coupling mechanism discussed above, which will clarify the similarities between RMn$_2$O$_5$ and other multiferroic materials. The positions of Mn^{3+} and Mn^{4+} in the paramagnetic unit cell are shown in table 1 and the eight vector order parameters can be found in table 2 (we use the notations of Bertaut *et al* [35]).

Table 3. Irreducible representations of the space group *Pbam* for $Q = (1/2, 0, 1/2)$.

	2_x	2_y	2_z	m_x	m_y	m_z	I
Γ_1	$\begin{pmatrix} 0 & 1 \\ -1 & 0 \end{pmatrix}$	$\begin{pmatrix} 1 & 0 \\ 0 & -1 \end{pmatrix}$	$\begin{pmatrix} 0 & -1 \\ -1 & 0 \end{pmatrix}$	$\begin{pmatrix} 1 & 0 \\ 0 & -1 \end{pmatrix}$	$\begin{pmatrix} 0 & 1 \\ -1 & 0 \end{pmatrix}$	$\begin{pmatrix} 1 & 0 \\ 0 & 1 \end{pmatrix}$	$\begin{pmatrix} 0 & -1 \\ -1 & 0 \end{pmatrix}$
Γ_2	$\begin{pmatrix} 0 & -1 \\ 1 & 0 \end{pmatrix}$	$\begin{pmatrix} 1 & 0 \\ 0 & -1 \end{pmatrix}$	$\begin{pmatrix} 0 & 1 \\ 1 & 0 \end{pmatrix}$	$\begin{pmatrix} -1 & 0 \\ 0 & 1 \end{pmatrix}$	$\begin{pmatrix} 0 & 1 \\ -1 & 0 \end{pmatrix}$	$\begin{pmatrix} -1 & 0 \\ 0 & -1 \end{pmatrix}$	$\begin{pmatrix} 0 & -1 \\ -1 & 0 \end{pmatrix}$

Table 4. Basis vectors of the space group *Pbam* for $Q = (1/2, 0, 1/2)$.

Γ_1	$\begin{pmatrix} F_x \\ C_x \end{pmatrix} \begin{pmatrix} C_y \\ F_y \end{pmatrix}$	$\begin{pmatrix} G_x \\ -A_x \end{pmatrix} \begin{pmatrix} -A_y \\ G_y \end{pmatrix}$	$\begin{pmatrix} C'_z \\ F'_z \end{pmatrix} \begin{pmatrix} G'_x \\ -A'_x \end{pmatrix} \begin{pmatrix} -A'_y \\ G'_y \end{pmatrix}$
Γ_2	$\begin{pmatrix} F_z \\ C_z \end{pmatrix}$	$\begin{pmatrix} G_z \\ -A_z \end{pmatrix} \begin{pmatrix} C'_x \\ F'_x \end{pmatrix} \begin{pmatrix} F'_y \\ C'_y \end{pmatrix}$	$\begin{pmatrix} G'_z \\ -A'_z \end{pmatrix}$

For a discussion of the phenomenological description of the magnetoelectric coupling, we have chosen the relatively simple case of $BiMn_2O_5$, which shows the commensurate spin ordering with $Q = (1/2, 0, 1/2)$. In this case the components of the order parameters belong to one of the two two-dimensional representations, Γ_1 or Γ_2, of the *Pbam* group (shown in table 3) [35, 48]. $BiMn_2O_5$ only shows the 'collinear' state with the a components of the Mn^{3+} and Mn^{4+} spins described, respectively, by the order parameters $F_x = -3.1\ \mu_B$ and $G'_x = 2.4\ \mu_B$ with small b components $C_y = -0.8\ \mu_B$ and $A'_y = 0.6\ \mu_B$ [48] corresponding to a small rotation between spins in neighbouring antiferromagnetic chains.

Since F_x is the part two-dimensional representation $\begin{pmatrix} F_x \\ C_x \end{pmatrix} \in \Gamma_1$, the state described by the order parameter C_x is another ground state of the system. These two states are related by inversion, which transforms F_x into $-C_x$ and vice versa. Based on the order parameters listed in table 4 and their transformation properties in table 3, it is easy to check that the magnetoelectric coupling of the form $-\lambda_x P_y (F_x^2 - C_x^2)$ is invariant upon all symmetry transformations of the paramagnetic phase, so that the order parameters F_x and C_x describe two ferroelectric states with opposite directions of electric polarization. It also easy to check that the couplings $-\lambda_y P_y (F_y^2 - C_y^2)$ and $-\lambda_z P_z (F_z^2 - C_z^2)$ are also allowed by symmetry, which is a strong indication that the mechanism inducing electric polarization in a magnetically ordered state is invariant upon the global spin rotation and the coupling can be written in the form $\lambda P_y (\mathbf{F}^2 - \mathbf{C}^2)$ [20].

Due to the exchange coupling between the Mn^{3+} and Mn^{4+} ions, the order parameters G'_x and F_x are strongly coupled. Since $\begin{pmatrix} G'_x \\ -A'_x \end{pmatrix}$ also belongs to the Γ_1 representation, the coupling between the two spin subsystems is phenomenologically described by $-g(F_x G'_x - C_x A'_x)$ [20]. Thus, more generally, the magnetoelectric coupling should be written in the form

$$\Phi_{me} = -\lambda P_y (\eta_1^2 - \eta_2^2), \tag{5}$$

where $\begin{pmatrix} \eta_1 \\ \eta_2 \end{pmatrix}$ belongs to the Γ_1 representation. This form of the third-order magnetoelectric coupling was discussed previously in the context of the orthorhombic manganites with the E-type magnetic ordering [22] and is typical for improper ferroelectrics [25].

4.4. Static and dynamic dielectric susceptibility

The contribution of the coupled spin–lattice degrees of freedom to static dielectric susceptibility is given by

$$\chi_1^{-1} \approx \left(\chi_1^{(0)} \right)^{-1} - \frac{1}{V} \sum_{i,j} I_i A_{ij}^{-1} I_j + \frac{1}{2V} \sum_{i,j} J''_{ij}(0)(\mathbf{S}_i \mathbf{S}_j), \tag{6}$$

where

$$A_{ij} = J_{ij}(\mathbf{S}_i \mathbf{S}_j) + \delta_{ij} \left[\sum_{\alpha=1,2} K_{i\alpha} \left(2(\mathbf{S}_i \hat{k}_{i\alpha})^2 - S_i^2 \right) - \sum_k J_{ik}(\mathbf{S}_i \mathbf{S}_k) \right] \tag{7}$$

and

$$I_i = \sum_j J'_{ij}[\mathbf{S}_i \times \mathbf{S}_j]_c, \tag{8}$$

The second term in (6) is the spin contribution to the dielectric constant due to virtual excitations of magnons by the electric field (this will become more apparent in the discussion of the dynamic susceptibility).

The last term in (6) describes the shift of the phonon frequency due to a change of the spring constants in magnetically ordered states. This effect is known in condensed matter spectroscopy as spin–phonon coupling [49, 50]. Phenomenologically, this effect is described by the fourth-order magnetoelectric coupling of the type $P^2 L^2$, where L is a magnetic order parameter. In most cases, magnon and phonon branches coupled through this term experience 'repulsion' and the phonon hardens. However, in the magnetically frustrated compounds, this contribution to the dielectric constant can have either sign and can result in either hardening or softening of phonons in the magnetic phase (see, e.g., [51] on $CdCr_2S_4$ spinel).

Equations of motion describing the coupled spin–lattice dynamics have the form

$$\ddot{P}_b = -\frac{\chi_0 \omega_0^2}{V} \frac{\partial H}{\partial P_b},$$

$$\dot{\mathbf{S}}_i = \left[\frac{\partial H}{\partial \mathbf{S}_i} \times \mathbf{S}_i \right], \tag{9}$$

where $\chi_0 = \chi_1^{(0)} + \chi_2$ and ω_0 is the bare frequency of the polar phonon. Omitting the fourth-order coupling term and solving linearized equations of motion, we obtain the dynamic dielectric susceptibility:

$$\chi^{-1}(\omega) \approx \chi_0^{-1}\left(1 - \frac{\omega^2}{\omega_0^2}\right)$$
$$- \frac{1}{V}\sum_{i,j} I_i \left[(BA - \omega^2)^{-1}B\right]_{ij} I_j, \qquad (10)$$

where

$$B_{ij} = J_{ij} + \frac{\delta_{ij}}{S_i^2}\sum_{\alpha=1,2}\left(K_{i\alpha}(\boldsymbol{S}_i\hat{k}_{i\alpha})^2 - K_{i3}S_i^2\right)$$
$$- \frac{\delta_{ij}}{S_i^2}\sum_k J_{ik}(\boldsymbol{S}_i\boldsymbol{S}_k). \qquad (11)$$

The second term in (10) describes the transfer of a part of the electric dipole spectral weight from phonon to magnon frequencies, which turns magnons coupled to phonons into electromagnons. If such an electromagnon has lower frequency than the phonon, the static dielectric constant $\varepsilon(0) = 1 + 4\pi\chi(0)$ increases as a result of the coupling showing a step-like anomaly. Furthermore, frequencies of the mixed spin–lattice excitations (poles of the dielectric susceptibility (10)) are shifted down with respect to the 'bare' magnon frequencies, found from

$$\det(BA - \omega^2) = 0. \qquad (12)$$

Note that the electromagnon term in (10) disappears for collinear spin states, as I_i, defined by (8), is zero in this case. This can be understood as follows. Classically, magnons correspond to spin oscillations that are orthogonal to ordered spin vectors. The change of the scalar product of a pair of collinear spins is then proportional to the second power of the amplitude of the oscillations. Since the magnetoelectric coupling in our model originates solely from Heisenberg exchange and only involves scalar products of spins, the linear coupling of electric field to magnons is absent for collinear spins and the lowest-order process is the photo-excitation of a pair of magnons.

In figures 9(a) and (b), we plot the real and imaginary parts of the dielectric function (dotted red and solid blue lines, respectively) for the 'high-temperature' and 'low-temperature' states shown in, respectively, figures 6(a) and (b) (the imaginary part was obtained by the shift $\omega \rightarrow \omega + i\frac{\gamma}{2}$ with $\gamma = 1$ K). As was explained above, the coupling of magnons to the electric component of light and a significant electric dipole absorption at magnon frequencies is only present in the non-collinear 'low-temperature' phase, in agreement with experiment. This result may seem somewhat counterintuitive: while the spontaneous electric polarization induced by the Heisenberg exchange striction is maximum for the collinear state, the excitation of magnons by the electric component of light (electromagnons) requires non-collinear spins and is only observed below the spin re-orientation transition.

The red points in figure 9 mark the bare frequencies of the softest magnons with zero wavevector, found from (12). Since the magnetic unit cell in this calculation contains 16 magnetic ions, the total number of such magnons is also 16. However,
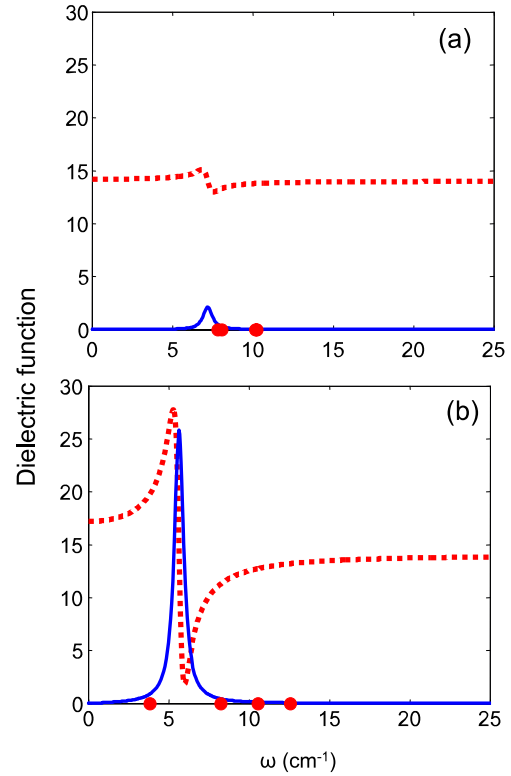

Figure 9. The model calculation results: frequency dependence of the real (ε_1) and imaginary (ε_2) parts of the dielectric function (dotted red and solid blue lines, respectively) for the 'high-temperature' collinear state (panel (a)) and the 'low-temperature' non-collinear state (panel (b)) shown, respectively, in panels (a) and (b) of figure 6. Red points are selected magnon frequencies of spins decoupled from the lattice found as the roots of (12). A magnon at 11.8 cm^{-1} couples to a polar phonon at 100 cm^{-1} and becomes an electromagnon observable as the peak of the ε_2.

only one of them is strongly coupled to the electric component of light and significantly contributes to the dielectric constant. This electromagnon corresponds to the relative rotation of spins of the neighbouring antiferromagnetic chains, which gives rise to oscillations of the induced electric polarization in the b direction. The frequency of this uncoupled magnon for the non-collinear spin configuration shown in figure 6(b) is 11.8 cm^{-1}. As the position of the absorption peak in figure 9(b) is clearly lower that this magnon frequency, our parameters correspond to the strong magnetoelectric coupling case. The strong coupling is apparently necessary, if the large difference between dielectric constants of the 'high'- and 'low'-temperature phases $\Delta\varepsilon'(0)$ (=3.25 in our calculation) is associated solely with the absorption peak emerging in the non-collinear state.

The results of our model calculations presented in figure 9(b) show that the symmetry properties of one magnon and the lattice allow an electromagnon in this system. Next, we discuss the strength of coupling. In our model, the first derivatives of the exchange integrals J_{ij} are the coupling constants. Both magnetically induced polarization and electromagnon were calculated using the same set of J' values. The characteristic value of J' used in our calculation

was $dJ_3/dy = 4$ meV Å^{-1} which is much less than, for example, 40 meV Å^{-1} for ZnCr$_2$O$_4$ [52].

5. Discussion

Our model calculations show that the observed values of the polarization and electromagnon strength are obtained with realistic symmetric exchange constants. Also, the electromagnon coupling has been shown to be of Heisenberg type by the observed selection rules. These are strong arguments in favour of the Heisenberg exchange origin of the polarization and electromagnons in the RMn$_2$O$_5$ family. However, in comparing the experimental and theoretical results, we should keep in mind that in the compounds of interest both symmetric and antisymmetric exchange mechanisms are operative and they both may produce polarization and electromagnons. Therefore, it is important to compare both the spontaneous polarization and the electromagnon selection rules in both RMnO$_3$ and RMn$_2$O$_5$ with these two mechanisms.

In particular, the origin of ferroelectricity in RMn$_2$O$_5$ remains controversial. An alternative to the magnetostriction scenario discussed here is electric polarization induced by the *bc* spiral, as observed in recent experiments [46, 47, 53] via the inverse Dzyaloshinskii–Moriya mechanism of relativistic origin [17, 18, 24]. One natural question is whether the electromagnon study can clarify this controversy.

Electromagnon excitations for the cycloidal spiral state were studied by Katsura *et al* [14]. According to their theory, the electric field of light that excites an electromagnon has to be orthogonal to the direction of the electric polarization induced by the spiral, which can be easily understood as follows. The spin spiral induces electric polarization that lies in the spiral plane and is orthogonal to the propagation wavevector of the spiral [24]. Thus the *bc* spiral in RMn$_2$O$_5$ with the wavevector along the *c* axis would induce polarization along the *b* axis, in agreement with experiment. An electric field applied in the direction perpendicular to the spiral plane will result in a small rotation of this plane, as a result of which the spontaneous polarization vector acquires a component parallel to the applied field. An oscillating electric field orthogonal to the spiral plane will then excite oscillations of this plane, which is precisely the electromagnon of Katsura *et al* [14]. Since the polarization lies in the spiral plane, the polarization of light should be orthogonal to the spontaneous polarization. Thus, to excite the oscillations of the *bc* spiral would require $e \parallel a$, whereas in the experiment the electric field is parallel to the *b* axis and the direction of electric polarization. Indeed, this can be an argument against the spiral scenario of multiferroicity of RMn$_2$O$_5$.

However, the situation is complicated by the fact that even in RMnO$_3$ compounds, where the spiral origin of the magnetically induced electric polarization is well established, the selection rule $e \perp P$ is not obeyed. This was demonstrated by optical measurements in the magnetic field. The magnetic field applied to DyMnO$_3$ [31] and TbMnO$_3$ [43] gives rise to the magnetic flop transition at which the *bc* spiral is replaced by the *ab* spiral. The spiral flop, however, has

no effect on the polarization of electromagnons, which are always observed for $e \parallel a$. Also in Eu$_{0.75}$Y$_{0.25}$MnO$_3$, where the spin spiral lies in the *ab* plane already for zero magnetic field and the induced electric polarization is parallel to *a*, the selection rule for electromagnons remains the same: $e \parallel a$ [29]. Therefore, the selection rules in both RMnO$_3$ and RMn$_2$O$_5$ are tied to the lattice, not the spin plane. The selection rule for RMnO$_3$ appears to originate from the GdFeO$_3$ distortions of the perovskite structure of orthorhombic manganites, which generates new types of magnetoelectric interactions and couples light to magnetic excitations that are different from the oscillations of the spiral plane [54]. Furthermore, these distortions may also couple to the zone edge magnons and account for the broad peak observed in RMnO$_3$ at high frequencies. However, an alternative mechanism for the broad peak is the photo-excitation of bi-magnons and so the precise origin of this high-frequency peak in RMnO$_3$ remains an open question.

In any case, it appears that electromagnons in RMnO$_3$ are also induced by symmetric exchange even though the spontaneous polarization is produced by the DM-type antisymmetric exchange mechanism. This is understood as a consequence of the vanishing of any static polarization induced by symmetric exchange due to the symmetry of the lattice [18]. Another important question then is why the antisymmetric exchange does not produce electromagnon excitations? We suspect that the relativistic interactions are just too weak to produce observable signals. The observation of these weak DM-induced electromagnons would help clarify the overall picture of spin–lattice interactions in multiferroics.

Consequently, while our experimental and theoretical results strongly suggest that the magnetoelectric coupling in RMn$_2$O$_5$ is governed by Heisenberg exchange, we cannot safely rule out the spiral scenario for the spontaneous polarization in these materials on the basis of optical data. However, the results of recent neutron scattering experiments [53] suggest rather that the spiral components appear as a consequence of the existence of spontaneous polarization.

6. Summary

We have presented experimental evidence and theoretical analysis that demonstrate that electromagnon excitations are present in both RMn$_2$O$_5$ and RMnO$_3$ multiferroics. These electric dipole mixed magnon–phonon modes are observed in the far-infrared and match excitations observed in inelastic neutron spectra in both classes of materials. The polarization selection rules observed in the infrared experiments show that the electromagnon excitations are generated only by symmetric exchange in both classes of materials. The observed selection rules are tied to the lattice, not the spin plane, in contrast to the predictions of the antisymmetric exchange model.

To theoretically account for electromagnons, we have considered third-and fourth-order coupling between the lattice and spins. The fourth-order terms produce spin–phonon interactions that lead to shifts of the magnon and phonon frequencies near magnetic phase transitions observed

in many magnetic materials. The third-order coupling terms can produce mixed magnon–phonon excitations—the electromagnons—only for non-collinear spin orders. The third-order terms are also responsible for the spontaneous polarization in multiferroics [6]. We also developed a simple microscopic model of RMn_2O_5 that explains the transition between collinear and non-collinear spin states, the magnetically induced electric polarization in the collinear state and the appearance of the electromagnon peak in the non-collinear state as well as the polarization of light for which this peak is observed. The mechanism of magnetoelectric coupling in this model relies entirely on isotropic Heisenberg exchange and magnetostrictive coupling of spins to a polar phonon mode.

Acknowledgments

References

[1] Smolenskii G A and Chupis I E 1982 *Sov. Phys.–Usp.* **25** 475
[2] Fiebig M 2005 *J. Phys. D: Appl. Phys.* **38** R123
[3] Prellier W, Singh M P and Murugavel P 2005 *J. Phys.: Condens. Matter* **17** R803
[4] Khomskii D I 2006 *J. Magn. Magn. Mater.* **306** 1
[5] Eerenstein W, Mathur N D and Scott J F 2006 *Nature* **442** 759
[6] Cheong S-W and Mostovoy M 2007 *Nat. Mater.* **6** 13
[7] Ramesh R and Spaldin N A 2007 *Nat. Mater.* **6** 21
[8] Kimura T, Goto T, Shintani H, Ishizaka K, Arima T and Tokura Y 2003 *Nature* **426** 55
[9] Hur N, Park S, Sharma P A, Ahn J S, Guha S and Cheong S-W 2004 *Nature* **429** 392
[10] Lawes G, Harris A B, Kimura T, Rogado N, Cava R J, Aharony A, Entin-Wohlman O, Yildirim T, Kenzelmann M, Broholm C and Ramirez A P 2005 *Phys. Rev. Lett.* **95** 087205
[11] Goto T, Kimura T, Lawes G, Ramirez A P and Tokura Y 2004 *Phys. Rev. Lett.* **92** 257201
[12] Pimenov A, Mukhin A A, Ivanov V Yu, Travkin V D, Balbashov A M and Loidl A 2006 *Nat. Phys.* **2** 97
[13] Sushkov A B, Valdés Aguilar R, Park S, Cheong S-W and Drew H D 2007 *Phys. Rev. Lett.* **98** 027202
[14] Katsura H, Balatsky A V and Nagaosa N 2007 *Phys. Rev. Lett.* **98** 027203
[15] Kimura T 2007 *Annu. Rev. Mater. Res.* **37** 387
[16] Moriya T 1960 *Phys. Rev.* **120** 91
[17] Katsura H, Nagaosa N and Balatsky A V 2005 *Phys. Rev. Lett.* **95** 057205
[18] Sergienko I A and Dagotto E 2006 *Phys. Rev. B* **73** 094434
[19] Jia C, Onoda S, Nagaosa N and Han J H 2007 *Phys. Rev. B* **76** 144424
[20] Kadomtseva A M, Krotov S S, Popov Yu F, Vorobev G P and Lukina M M 2005 *JETP* **100** 305
[21] Chapon L C, Radaelli P G, Blake G R, Park S and Cheong S-W 2006 *Phys. Rev. Lett.* **96** 097601
[22] Sergienko I A, Sen C and Dagotto E 2006 *Phys. Rev. Lett.* **97** 227204
[23] Bary'achtar V G, L'vov V A and Jablonskii D A 1983 *JETP Lett.* **37** 673
[24] Mostovoy M 2006 *Phys. Rev. Lett.* **96** 067601
[25] Levanyuk A P and Sannikov D G 1974 *Sov. Phys.–Usp.* **17** 199
[26] Lorenzana J and Sawatzky G A 1995 *Phys. Rev. Lett.* **74** 1867
[27] Damascelli A, van der Marel D, Grüninger M, Presura C, Palstra T T M, Jegoudez J and Revcolevschi A 1998 *Phys. Rev. Lett.* **81** 918
[28] Pimenov A, Rudolf T, Mayr F, Loidl A, Mukhin A A and Balbashov A M 2007 *Phys. Rev. B* **74** 100403
[29] Valdés Aguilar R, Sushkov A B, Zhang C L, Choi Y J, Cheong S-W and Drew H D 2007 *Phys. Rev. B* **76** 060404(R)
[30] Pimenov A, Loidl A, Mukhin A A, Travkin V D, Ivanov V Yu and Balbashov A M 2008 *Phys. Rev. B* **77** 014438
[31] Kida N, Ikebe Y, Takahashi Y, He J P, Kaneko Y, Yamasaki Y, Shimano R, Arima T, Nagaosa N and Tokura Y 2007 *Preprint* 0711.2733
[32] de Sousa R and Moore E J 2008 *Phys. Rev. B* **77** 012406
[33] de Sousa R and Moore E J 2008 *Appl. Phys. Lett.* **92** 022514
[34] Fang C and Hu J 2008 *Europhys. Lett.* **82** 57005
[35] Bertaut E F, Buisson G, Quezel-Ambrunaz S and Quezel G 1967 *Solid State Commun.* **5** 25
[36] Harris A B, Aharony A and Entin-Wohlman O 2008 *Phys. Rev. Lett.* **100** 217202
[37] Sanina V A, Sapozhnikova L M, Golovenchits E I and Morozov N V 1988 *Sov. Phys.–Solid State* **30** 1736
[38] Mukhin A A, Travkin V D, Ivanov V Yu, Lebedev S P, Prokhorov A S and Kon K 2001 *Bull. Lebedev Phys. Inst.* **4** 34
[39] Golovenchits E I and Sanina V A 2003 *JETP Lett.* **78** 88
[40] Kuzmenko A B 2004 Reffit: Software to fit optical spectra http://optics.unige.ch/alexey/reffit.html
[41] Kobayashi S, Osawa T, Kimura H, Noda Y, Kagomiya I and Kohn K 2004 *J. Phys. Soc. Japan* **73** 1031
[42] Sirenko A A, O Malley S M, Ahn K H, Park S, Carr G L and Cheong S-W 2007 *Preprint* cond-mat/0703255v1
[43] Valdés Aguilar R 2008 *PhD Thesis* University of Maryland
[44] Lee S-H, Kim J H, Chung J-H, Qiu Y, Kenzelmann M, Sato T J, Park S Y and Cheong S-W 2007 *Bull. Am. Phys. Soc.* **52** 330
[45] Senff D, Link P, Hradil K, Hiess A, Regnault L P, Sidis Y, Aliouane N, Argyriou D N and Braden M 2007 *Phys. Rev. Lett.* **98** 137206
[46] Noda Y, Kimura H, Kamada Y, Osawa T, Fukuda Y, Ishikawa Y, Kobayashi S, Wakabayashi Y, Sawa H, Ikeda N and Kohn K 2006 *Physica* B **385–386** 119–22
[47] Vecchini C, Chapon L C, Brown P J, Chatterji T, Park S, Cheong S-W and Radaelli P G 2008 *Phys. Rev. B* **77** 134434
[48] Muñoz A, Alonso J A, Casais M T, Martínez-Lope M J, Martínez J L and Fernández-Díaz M T 2002 *Phys. Rev. B* **65** 144423
[49] Baltensperger W and Helman J S 1968 *Helv. Phys. Acta* **41** 668
[50] Sushkov A B, Tchernyshyov O, Ratcliff W II, Cheong S-W and Drew H D 2005 *Phys. Rev. Lett.* **94** 137202
[51] Wakamura K and Arai T 1988 *J. Appl. Phys.* **63** 5824
[52] Lee S-H, Broholm C, Kim T H, Ratcliff W II and Cheong S-W 2000 *Phys. Rev. Lett.* **84** 3718
[53] Kim T H *et al* 2008 *Preprint* 0803.1123v2
[54] Mostovoy M *et al* 2008 at press